Mesoporous Beta zeolites with controlled distribution of Brønsted acid sites for alkylation of benzene with cyclohexene

Results in Engineering 19 (2023) 101377

Contents lists available at ScienceDirect

Results in Engineering

journal homepage: www.sciencedirect.com/journal/results-in-engineering

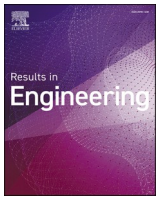

Mesoporous Beta zeolites with controlled distribution of Brønsted acid sites for alkylation of benzene with cyclohexene

Yeqing Huang [a,c], Manna Wang [a,b], Yi Huang [d], Jin Shang [e,f], Baoyu Liu [a,b,*]

[a] School of Chemical Engineering and Light Industry, Guangdong University of Technology, Guangzhou, 510006, China
[b] Jieyang Branch of Chemistry and Chemical Engineering Guangdong Laboratory (Rongjiang Laboratory), Jieyang, 515200, China
[c] Shenzhen Pingshan District Emergency Management Bureau, Shenzhen, 518118, China
[d] School of Engineering, Institute for Materials & Processes, The University of Edinburgh, Robert Stevenson Road, Edinburgh, EH9 3FB, United Kingdom
[e] School of Energy and Environment, City University of Hong Kong, Hong Kong, China
[f] City University of Hong Kong Shenzhen Research Institute, Shenzhen, China

ARTICLE INFO

Keywords:
Brønsted acid sites
Beta zeolites
Cyclohexylbenzene
Alkylation

ABSTRACT

The distribution of Brønsted acid sites in three-dimensional 12-membered pore channels of Beta zeolite was a decisive factor in the alkylation of benzene with cyclohexene. Here, the Brønsted acid site distribution in Beta zeolitic channels was precisely regulated by tuning the content of Na^+ in crystallization system combined with tetraethylammonium cation, the Beta-55 with Brønsted acid sites exclusively located in straight channels (along *a*- and *b*-axis directions) was successfully synthesized by utilizing tetraethylammonium as the structure-directing agents without Na^+ species, and the fraction of Brønsted acid sites in sinusoidal/straight channels of Beta zeolites can be accurately controlled by tailoring the content of Na^+ in synthesis gel. Catalytic properties in the liquid alkylation between benzene and cyclohexene exhibited that Beta-55 zeolites with the Brønsted acid sites solely located in *a*-axis and *b*-axis channels showed the highest cyclohexene conversion, cyclohexylbenzene selectivity and longest lifetime in this reaction. In addition, the resultant Beta zeolites also exhibited low coke generation rate and robust regeneration performance in the alkylation reaction.

1. Introduction

Cyclohexylbenzene (CHB) is a high value-added fine chemical with a freezing point close to room temperature and a high boiling point [1], which can be used in the production of high-boiling solvents, high-end plastics, scintillator and blends in diesel fuel [2]. Cyclohexylbenzene can also be used as a protectant in lithium-ion secondary batteries to prevent overcharge of the battery [3–5]. The CHB is produced by alkylation of benzene with cyclohexene, which is performed based on the conventional homogeneous catalysts including hydrofluoric acid, anhydrous aluminum chloride, and $Sc(OTf)_3$. Although these catalysts exhibit good performance in the synthesis of cyclohexylbenzene, they also bring into serious issues such as equipment corrosion, environmental pollution, difficulty in separation [6,7]. Therefore, it's highly desired to explore an efficient and eco-friendly solid acid catalytic technology for the production of cyclohexylbenzene.

Beta zeolite is a promising solid catalyst in the preparation of cyclohexylbenzene, it has a three-dimensional 12-membered ring (MR) interleaved pore structure with straight pores of 6.6 × 6.7 Å diameter in the *a*-axis and *b*-axis directions, and a curved pore of 5.6 × 5.6 Å diameter in the *c*-axis direction that crosses the *a*-axis and *b*-axis [8,9]. The kinetic diameters of benzene and cyclohexene are ~5.6 Å and ~6.2 Å [10], respectively, thus the benzene molecules can diffuse in all 12 MR channels of Beta zeolite while cyclohexene can only diffuse in the *a*-axis and *b*-axis channels of Beta zeolite. The kinetic diameter of cyclohexylbenzene is ~6.7 Å [11], which is matched with the pore size of Beta zeolite in the *a*-axis and *b*-axis directions, so the Beta zeolite possesses shape-selectivity towards cyclohexylbenzene.

For aluminosilicate zeolites, the acidic sites of zeolites are highly correlated with the aluminum atoms in the framework [12,13]. Aluminum atoms can occupy different positions within the zeolite framework, which influences the distribution of acidic sites. For the alkylation between benzene and cyclohexene catalyzed by Beta zeolites, the distributions of benzene and cyclohexene molecules in *a*-axis, *b*-axis and *c*-axis channels of Beta zeolites are different based on the above analysis, which reduces the alkylation efficient and causes the repaid

* Corresponding author. School of Chemical Engineering and Light Industry, Guangdong University of Technology, Guangzhou, 510006, China.
E-mail address: baoyu.liu@gdut.edu.cn (B. Liu).

https://doi.org/10.1016/j.rineng.2023.101377
Received 16 July 2023; Received in revised form 12 August 2023; Accepted 23 August 2023
Available online 1 September 2023

deactivation of Beta zeolites because of the existence of unwanted Brønsted acid sites in the *c*-axis channels for the alkylation reaction [14–16]. As a consequence, the distribution of acidic sites within Beta zeolites should be delicately tuned by manipulating the location of aluminum atoms in the framework [17]. The acidity of Beta zeolite is highly correlated with the T atom of framework, and the acidic sites of Beta zeolite can be regulated by in situ and post-treatment methods, such as: dealumination, construction of hierarchical porosity, surface passivation, tuning Si/Al ratio and embedding heteroatoms [18–26]. However, these techniques are difficult to precisely control the distribution of acidic sites in different pore channels of Beta zeolites, which impedes its application in the synthesis of cyclohexylbenzene.

In this study, a facile strategy is designed to prepare hierarchical Beta zeolites with precisely controlled distribution of Brønsted acid sites in the *a*-, *b*- and *c*-axis channels of Beta zeolites, in which the ratio of TEA^+ and Na^+ is modulated by tuning the contents of sodium chloride in the synthetic precursors to regulate the distribution of $[AlO_4]^-$species in Beta zeolites, it in turn controls the distribution of Brønsted acid sites in the 12-MR channels of Beta zeolites. In addition, the catalytic properties of prepared Beta zeolites are investigated in the liquid-phase alkylation between benzene with cyclohexene. It's observed that the Beta zeolites with Brønsted acid sites mainly distributed within the *a*-axis and *b*-axis pore channels not only improve the catalytic activity of alkylation reactions, but also restrict the self-polymerization of cyclohexene and improve the selectivity of alkylation products. Furthermore, it's found that the Beta zeolites with Na^+ free system is benefit to reducing the coke deposition, which is essential for the practical utilization of Beta zeolites in alkylation reaction of benzene and cyclohexene.

2. Experiment

2.1. Materials

Fumed silica (SiO_2, Aladdin), Sodium chloride (99.5%, Damao), aluminum isopropoxide (99.8%, Macklin), cetyltrimethylammonium bromide (99%, Macklin), tetraethylammonium hydroxide (35% in H_2O, Energy Chemical), benzene (99.5%, Macklin), cyclohexene (99%, Macklin), n-decane (99%, Macklin), deionized water, pyridine (AR, Macklin) and 2,4,6-Trimethylpyridine (99%, Macklin) were used. All reagents in this experiment were commercial reagents and used directly.

2.2. Synthesis of catalysts

Hierarchical Beta zeolites with precisely controlled Brønsted acid sites were synthesized by a simple one-step method. In a representative preparation: 23.14 g of TEAOH, 13.77 g of H_2O and a certain amount of NaCl were stirred uniformly in a beaker at 298 K until the solid was dissolved, then the temperature was raised to 333 K, 1.06 g of aluminum isopropoxide was added to the above solution and dissolved it under stirring, 1.42 g of CTAB (cetyltrimethylammonium bromide) was added sequentially, finally 6.0 g of fumed silica was slowly added under vigorous stirring, and then continued stirring for 4 h at 298 K. The resulting gel with an ultimate molar composition of 100 SiO_2: 5.2 Al_2O_3: 55 TEAOH: 3.9 CTAB: *x* NaCl: 1600 H_2O ($x = 0$, 1, 3, and 6, respectively) was poured into a stainless steel autoclave lined with Teflon and reacted at 423 K for 188 h under a static environment. The reacted autoclave was cooled and then the obtained Beta zeolites were centrifugally washed to pH neutrality and finally dried at 373 K for 4 h. Finally, these Beta zeolites were subjected to calcination at 823 K for 5 h, and the resultant samples were denominated as Beta-55-*x*NaCl depending on the amount of NaCl ($x = 0$, 1, 3, and 6, respectively).

2.3. Catalyst characterization

The crystal structures of the prepared zeolites were characterized by X-ray diffraction instrumentation equipped with a Brucker D8 Advance diffractometer with Cu Kα radiation. The pore structure parameters of Beta zeolites were measured by Micromeritics ASAP 2460 devices at 77 K. Zeolite were pretreated under the condition of 473 K and vacuum for 6 h. The total surface area of the resulting samples was determined by the Brunauer-Emmett-Teller (BET) model, while the pore size distribution was obtained by the Barrett−Joyner−Halenda model based on N2 desorption isotherm. The crystal morphology of the samples was achieved on a ZEISS Gemini 500 devices. The total acidity and external acidity were determined by Fourier transform infrared spectroscopy with the probe molecules of pyridine and 2,4,6-Trimethylpyridine, respectively, using a Bruker VERTEX 70 spectrometer. The zeolites were first degassed at 723 K for 2 h before the measurements, Pyridine or 2,4,6-Trimethylpyridine molecules were then adsorbed on the above zeolites for 0.5 h at 298 K. The temperature of the sample was raised to 423 K 1 h to get rid of the weakly bound pyridine molecules. After the samples were cooled to 298 K, the acidity of zeolites was measured by infrared spectroscopy at 30 scans and a resolution of 2 cm^{-1}. In the Py-IR spectra, the characteristic peak of Brønsted acid sites of zeolite is at ~1545 cm^{-1}, corresponding to a molar extinction coefficient of 2.22 cm/μmol. In the 3MPy-IR spectra, the characteristic peak of Brønsted acid sites inside the pore channel along the *a*- and *b*-axis directions is at ~1636 cm^{-1}, corresponding to a molar extinction coefficient of 10.1 cm/μmol, the amount of acidity of samples were calculated according to our previous report [28]. The Si/Al ratios of zeolites were determined by inductively coupled plasma optical emission spectroscopy (ICP-OES) using an Agilent 720 ES. Thermogravimetric analyses (TG) were used to determine the coke content on Beta zeolite after the reaction, and measurements were carried out in a STA449F5 device. The samples were gradually increased in temperature from 298 K to 1073 K at a ramp rate of 10 K min^{-1} under an air flow rate of 60 mL min^{-1}.

2.4. Catalytic tests

The catalytic properties of synthesized Beta zeolites were evaluated by alkylation of benzene with cyclohexene in a micro-fixed-bed reactor with an inner tube diameter of 10 mm at atmospheric pressure and 353 K, and the catalyst was pelletized with a size of 20–30 mesh. Prior to reaction, the resultant Beta zeolites with additional Na + species were ion exchanged three times with 1 M NH4NO3 solution at 353 K for 12 h. All catalysts were activated at 393 K for 12 h preceding the alkylation test. The benzene-olefin molar ratio in the reactants was 20:1, and *n*-decane was employed as an internal standard agent for quantification. The total weight hourly space velocity (WHSV) was 2 h^{-1} or 12 h^{-1}. The mixture after the reaction was regularly captured from the reactor piping and characterized using a gas chromatograph equipped with an HP-5 column and an FID detector. The conversion of cyclohexene and the selectivity of cyclohexylbenzene (CHB) were computed as follow:

$$\text{Conversion of Cyclohexene} = \left(1 - \frac{C_A}{C_{A0}}\right) \times 100\% \quad \text{(Eq.1)}$$

$$\text{Selectivity of CHB} = \left(\frac{n_{CHB}}{n_{CHB} + 2n_{DCHB} + 2n_{TCD}}\right) \times 100\% \quad \text{(Eq.2)}$$

where $C_{A,0}$ was the incipient cyclohexene concentration (mmol L^{-1}) and C_A was the concentration of cyclohexene (mmol L^{-1}) at reaction time t. The n_{CHB}, n_{DCHB} and n_{TCD} was the molar quantities of cyclohexylbenzene, dicyclohexylbenzene, and tricyclo[6,4,0,0(2,7)]dodecane, respectively. Catalyst regeneration was performed for spent Beta-55 or Beta-55-6NaCl in a muffle furnace with an air atmosphere. The ramp-up procedure was as described below: the temperature was increased from 323 K to 823 K at a ramp rate of 2 K min-1 and kept at 823 K for 5 h. The resultant zeolites were named as Regenerated Beta-55 or Regenerated Beta-55-6NaCl.

3. Results and discussion

3.1. Characterization of zeolite

The powder XRD patterns of Beta-55 and Beta-55-*x*NaCl samples were presented in Fig. 1. It was seen that all catalysts exhibited the characteristic diffraction peaks of BEA topology at 2θ = 7.6° and 22.5° [27], and these diffraction peaks also matched with the that of the 'standard' database as shown in the bottom of Fig. 1 (red line), indicating that typical Beta zeolites were successfully prepared. Meanwhile, the resultant Beta zeolites also showed similar diffraction intensities, suggesting that the additional sodium chloride had no obvious effect on the crystallinity of these samples.

The SEM images of all Beta zeolite samples were displayed in Fig. 2. In the absence of sodium cations, Beta-55 exhibited regular ellipsoidal morphology with aggregated nanocrystals, and the average size of aggregated nanocrystals was ~27 nm. When sodium cations were added into the synthesis system (SiO_2: NaCl = 100 : 1), Beta-55-1NaCl particles became irregular with a slight increase in nanocrystal size (~34 nm). While the Beta-55-3NaCl sample was composed of a stack of dense nanocrystals, and the Beta-55-6NaCl sample exhibited an obvious irregular aggregate due to the rapid growth of zeolite crystals in random directions arising from excessive Na^+, which can accelerate the nucleation under the structure directing effect, leading to the changes of zeolitic morphology.

The results of N_2 adsorption-desorption isotherms for all Beta zeolite samples were presented in Fig. 3a. It was evident that the adsorption of N_2 increased markedly at low relative pressure $P/P_0 < 0.05$ for all Beta zeolites, which corresponded to micropore adsorption of Beta zeolites, and the N_2 adsorption increased rapidly for all samples accompanied by a hysteresis loop at relative pressure $P/P_0 > 0.85$, which was assigned to the mesopores of stacking zeolite nanoparticles. The BJH pore size distributions of all samples were displayed in Fig. 3b, it was observed that all Beta zeolites possessed obvious bimodal mesopores, the small mesopores (3–4 nm) were intracrystalline mesopores produced by CTAB micelles [28], while the large mesopores (20–30 nm) were attributed to intercrystalline mesopores resulting from crystal stacking.

Table 1 showed the detailed textural properties of Beta-55 and Beta-55-*x*NaCl samples. Beta-55 possessed the highest total BET surface area, indicating that the additional sodium chloride in the synthesis system was not favorable for improving the surface area of zeolites, and Beta-55-3NaCl and Beta-55-6NaCl with nano-sized morphology exhibited enhanced total and mesoporous volumes due to their abundant mesopores generated by the stacking of nano-sized zeolites.

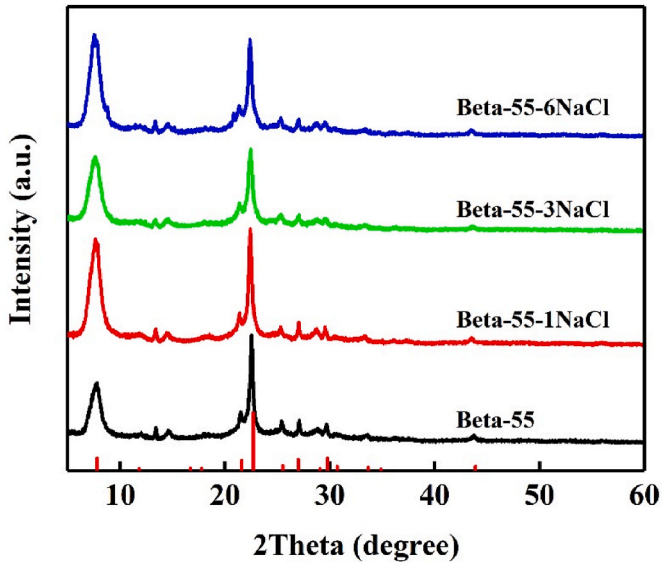

Fig. 1. XRD patterns of resultant catalysts.

3.2. Tuning the distribution of Brønsted acid sites for beta zeolites

Aluminum is the main source of acidic sites in aluminosilicate zeolites, and the distribution of aluminum atoms in tetrahedral sites directly determines the location of Brønsted acid sites (Si–OH–Al) of Beta zeolites, which are crucial for the alkylation of benzene with cyclohexene based on the aforementioned analysis. Here, the FT-IR (Fourier Transform Infrared) spectra of adsorbed different organic base were employed to identify the distributions of Brønsted acid sites for obtained Beta zeolites. The molecular size of pyridine is ~5.4 Å [29,30], which is smaller than the size of the 12 MR pore channel of Beta zeolite, so pyridine molecules can enter into all channel along the *a*-axis, *b*-axis and *c*-axis directions of Beta zeolites, and determining the total Brønsted acid sites of resultant catalysts. While the 2,4,6-trimethylpyridine (Me_3Py) has a large molecular size (6.2 × 5.6 Å) that can only access the pore channel along *a*-axis and *b*-axis of Beta zeolites (6.6 × 6.7 Å) [31–33], which is employed to detect the Brønsted acid sites exclusively located in the 12-MR channels along the *a*-axis and *b*-axis of Beta zeolites. In general, the FT-IR band of 1545 cm^{-1} is the adsorption of pyridine at the Brønsted acid site of Beta zeolite [34], while the FT-IR band of 1636 cm^{-1} is assigned to the adsorption of 2,4,6-trimethylpyridine at the Brønsted acid site of Beta zeolite [35]. The FT-IR spectra of H-form Beta-55 and Beta-55-xNaCl samples adsorbed with pyridine and 2,4,6-trimethylpyridine were displayed in Fig. 4a and b, respectively, and the Brønsted acidity of resultant Beta zeolites were summarized in Table 2.

It is found from Table 2 that the Brønsted acid sites in the *a*- and *b*-axis directions of Beta-55 accounted for 99% of the total Brønsted acid sites, indicating that the Brønsted acid sites mainly located in the 12 MR channels along *a*- and *b*-axis for Beta-55 without Na^+ species, because the large TEA^+ can only entered the 12 MR channels along *a*- and *b*-axis of Beta zeolites, as observed in Scheme 1, in which the positive TEA^+ interact with negative $[AlO_4]^-$, resulting in high proportion of Brønsted acid sites in the 12 MR channels along *a*- and *b*-axis directions for Beta-55. In contrast, the Na^+ with a ~0.19 nm diameter can freely diffuse in all three-dimensional 12-MR channels of Beta zeolites along the *a*-, *b*- and *c*-axis directions [36] (Scheme 1).

When the Na^+ species were added to the synthesis gel of Beta zeolites, it expected to tune the distribution of Brønsted acid sites in 12-MR channels of Beta zeolites. As can be seen from Table 2, with increasing Na^+ species in the synthesis system, the Brønsted acid sites along the *a*- and *b*-axis directions were decreasing, and a part of Brønsted acid sites moved into the *c*-axis direction of Beta zeolites since the small Na^+ can enter the pore channel along *c*-axis direction of Beta zeolite, which can interact with the negative $[AlO_4]^-$ species through the charge balance, resulting in the decrease of proportion of Brønsted acid sites in the pore channels along *a*- and *b*-axis directions for Beta-55-*x*NaCl. Based on the above analysis, the proposed steric hindrance effect between TEA^+/Na^+ and three-dimensional 12-membered ring pore channels of Beta zeolite along the *a*-, *b*- and *c*-axis directions combined with $[AlO_4]^-$ species based on charge balance interaction was presented in Scheme 2, which clearly illustrated the regulation mechanism of Brønsted acid site distributions along *a*-, *b*- and *c*-axis directions of Beta zeolites.

3.3. The catalytic performances of resultant catalysts

The catalytic performances of resultant Beta-55 and Beta-55-*x*NaCl samples in the alkylation of benzene with cyclohexene were investigated under harsh reaction condition (WHSV = 12 h^{-1}), as displayed in Fig. 5. It was evident that the activity of Beta zeolites increased in the order of Beta-55-6NaCl ≈ Beta-55-3NaCl < Beta-55-1NaCl < Beta-55, because the alkylation reaction mainly occurred in the *a*-axis and *b*-axis channels of Beta zeolites owing to the steric hindrance effect of large cyclohexene,

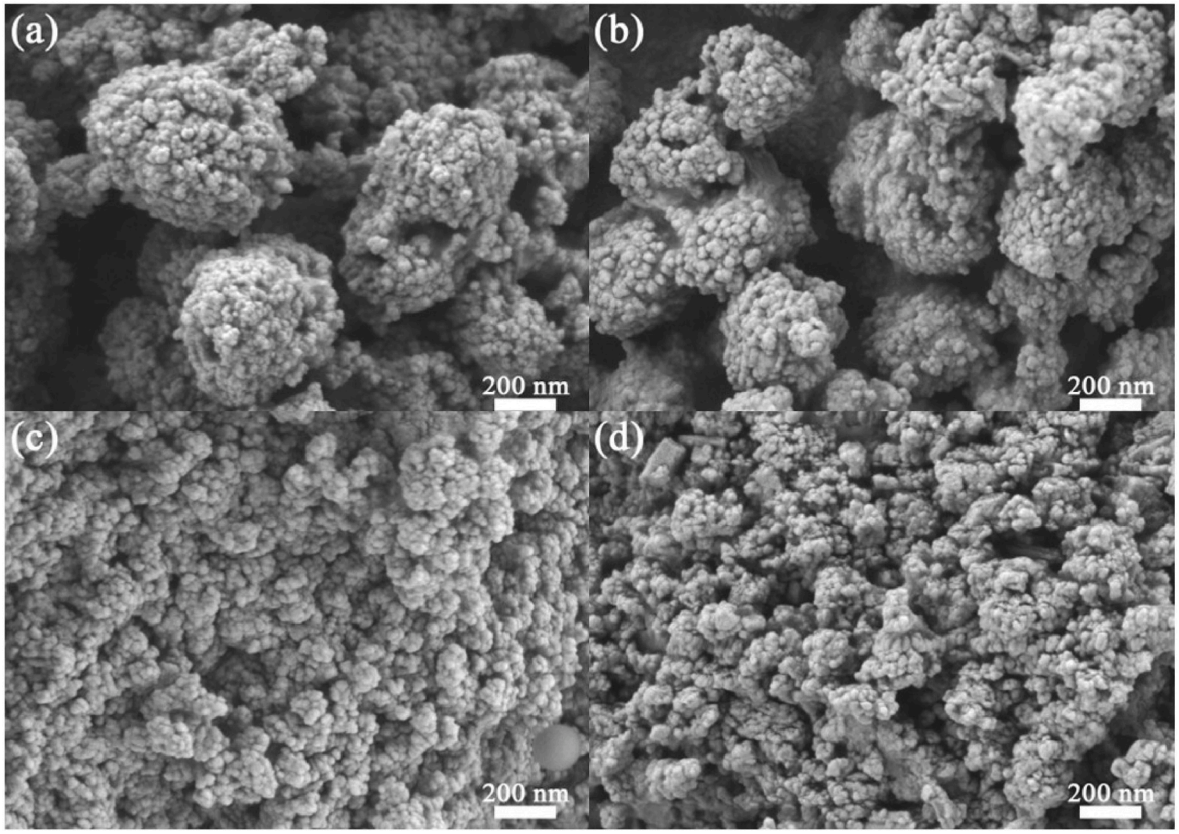

Fig. 2. SEM images of (a) Beta-55, (b) Beta-55-1NaCl, (c) Beta-55-3NaCl, and (d) Beta-55-6NaCl, respectively.

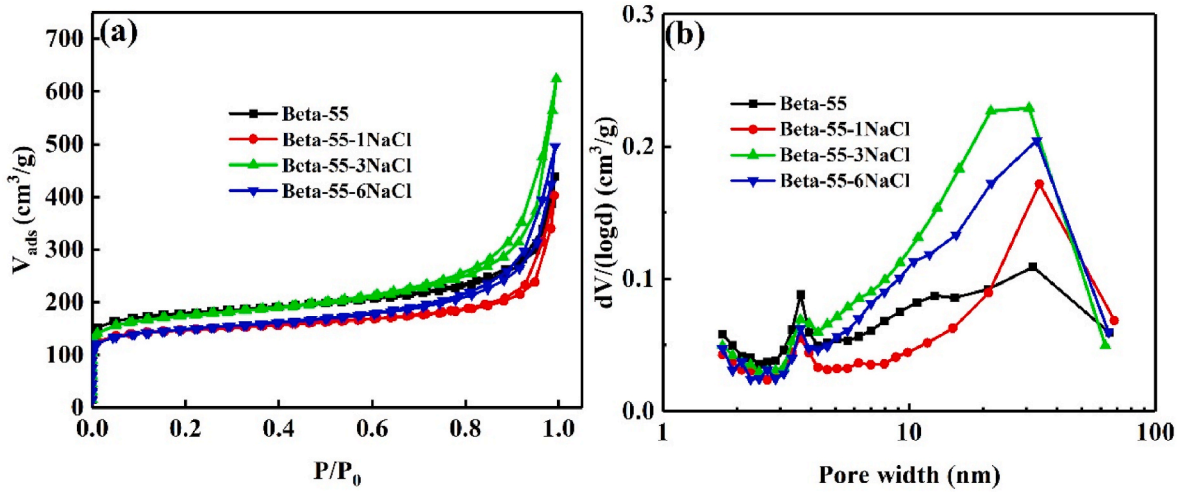

Fig. 3. N_2 adsorption-desorption isotherms (a) and BJH pore size distributions (b) of Beta zeolites.

it was favorable to increase the catalytic activity of Beta zeolites in the alkylation reaction through promoting the fraction of Brønsted acid sites in *a*-axis and *b*-axis channels of Beta zeolites, which was consistent with the acid data (Table 2). More interestingly, the Beta-55 also exhibited the highest selectivity of cyclohexylbenzene (CHB), indicating that the side reaction such as self-polymerization of cyclohexene and over-alkylation of cyclohexylbenzene were effectively inhibited through modulating the distribution of Brønsted acid sites and enhancing diffusion based on the contribution of mesopores.

On the one hand, it can suppress the self-polymerization of cyclohexene by increasing benzene/cyclohexene ratio that was achieved by reducing the faction of Brønsted acid sites in *c*-axis channel of Beta zeolites, which can release the benzene molecules that was absorbed by Brønsted acid sites located in *c*-axis channel, the released benzene molecules re-entered *a*- and *b*-axis channels, increasing the molar ratio of benzene and cyclohexene in the *a*- and *b*-axis channels of Beta zeolites, as presented in Scheme 3. On the other hand, the advanced bimodal mesopores can greatly intensify the diffusion of guest molecules in the channels of Beta zeolites, which accelerated the transport of cyclohexylbenzene and moved them out of the interior of zeolitic framework as soon as possible, inhibiting the occurrence of over-alkylation of CHB, resulting in high selectivity of CHB. In addition, the Beta-55 also exhibited the longest lifetime since the 99% Brønsted acid sites located in the *a*- and *b*-axis channels of Beta zeolites, which greatly

Table 1
Textural properties of resultant catalysts.

Zeolites	Si/Al[a]	S_{BET}[b] [m^2g^{-1}]	S_{ext} [m^2g^{-1}]	S_{micro} [m^2g^{-1}]	V_{tol}[c] [cm^3g^{-1}]	V_{micro}[d] [cm^3g^{-1}]	V_{meso}[e] [cm^3g^{-1}]
Beta-55	15	682	168	514	0.461	0.204	0.246
Beta-55-1NaCl	12	566	133	433	0.623	0.171	0.452
Beta-55-3NaCl	13	651	211	440	0.965	0.177	0.788
Beta-55-6NaCl	10	556	168	388	0.768	0.156	0.612

[a] Si/Al ratio of samples was determined by ICP-OES.
[b] Total surface of area was calculated by BET model.
[c] Based on adsorbed volume at $P/P_0 = 0.99$.
[d] Identified from t-plot model.
[e] $V_{meso} = V_{tol} - V_{micro}$.

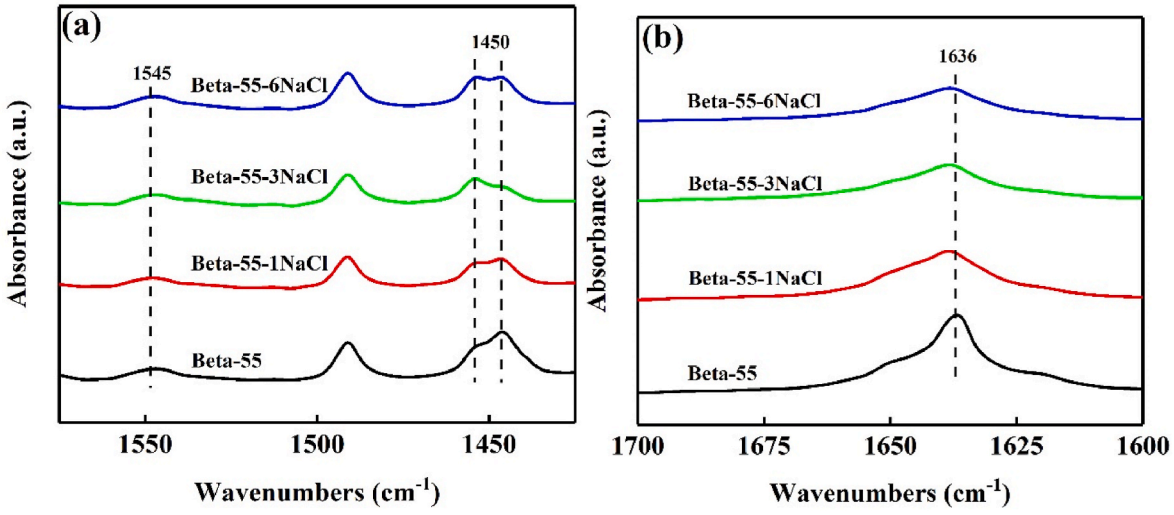

Fig. 4. FT-IR spectra of H-form Beta zeolites adsorbed with pyridine (a) and 2,4,6-trimethylpyridine (b).

Table 2
The distribution of Brønsted acidity in Beta zeolites.

Catalysts	C_{tolal}[a] (mmol/g)	$C_{a,b}$[b] (mmol/g)	C_c[c] (mmol/g)	[($C_{a,b}/C_{total}$) × 100%]
Beta-55	0.101	0.0995	0.0015	99%
Beta-55-1NaCl	0.082	0.0487	0.0333	59%
Beta-55-3NaCl	0.077	0.0379	0.0391	49%
Beta-55-6NaCl	0.088	0.0361	0.0519	41%

[a] The total concentration of Brønsted acid sites measured by FT-IR spectra of adsorbed pyridine.
[b] The concentration of Brønsted acid sites in the *a*- and *b*-axis directions measured by FT-IR spectra of adsorbed 2,4,6-Trimethylpyridine.
[c] C_c is the concentration of Brønsted acid sites in the *c*-axis direction, $C_c = C_{tolal} - C_{a,b}$.

inhibit the self-polymerization of cyclohexene based on the above analysis, leading to excellent stability.

Moreover, the catalytic properties of typical Beta-55 and Beta-55-6NaCl in the alkylation of benzene with cyclohexene were also tested under moderate condition (WHSV = 2 h^{-1}), as illustrated in Fig. 6, in which they both exhibited enhanced activity under mild reaction condition compared with harsh reaction condition (Fig. 5), and it was found from Fig. 6a and b that the selectivity of CHB gradually decreased with time on stream, while the selectivity of tricyclo[6,4,0,0(2,7)]dodecane (TCD) smoothly increased with time on stream, which can be reasonably ascribed to the fact that the coke species slowly deposited on the surface of Beta zeolites with time on stream, and they can accumulate in the channels of zeolites and further block the pores of Beta zeolites, which decreased the alkylation efficient and improved probability of self-polymerization of cyclohexene owing to the limited diffusion, resulting in the decrease of CHB selectivity with reaction time, which was consistence with the data as presented in Fig. 5.

The thermogravimetric analysis (TGA) was performed on the spent Beta zeolites and the results were shown in Fig. 7, it was observed from Fig. 7 that all samples exhibited three weight loss, the mass loss between 298 K and 423 K was ascribed to the removal of adsorbed moisture, while the mass loss between 423 K and 593 K was predominantly caused by the oxidative decomposition of soft coke arising from the occluded reactants and products, and the mass loss between 593 K and 1073 K was ascribed to the hard coke.

The detailed coke results of spent catalysts were given in Table 3, it could be noticed that Beta-55 showed the highest hard coke and the smallest amount of soft coke, because Beta-55 experienced the longest reaction time (Fig. 5), which was inclined to accumulating more hard coke in the channels of Beta zeolites, and some soft coke were easily transformed into hard coke with extending reaction time. However, the coke generation rate of resultant Beta zeolites decreased in the order of Beta-55-6NaCl > Beta-55-3NaCl > Beta-55-1NaCl > Beta-55, indicating that tuning the distribution of Brønsted acid sites in the 12 MR pore channels of Beta zeolite was crucial to extending the lifetime of catalysts in the alkylation of benzene with cyclohexene, it was benefit to extend the lifetime of Beta zeolites by increasing the fraction of Brønsted acid sites located in channels along *a*-axis and *b*-axis of Beta zeolites with large pore size (6.6 × 6.7 Å), which not only inhibited the self-polymerization of cyclohexene based on the aforementioned analysis but also facilitated the transfer of coke precursors from interior to the outside of zeolites through the large pore, resulting in enhanced stability.

To investigate the regeneration performance of obtained Beta

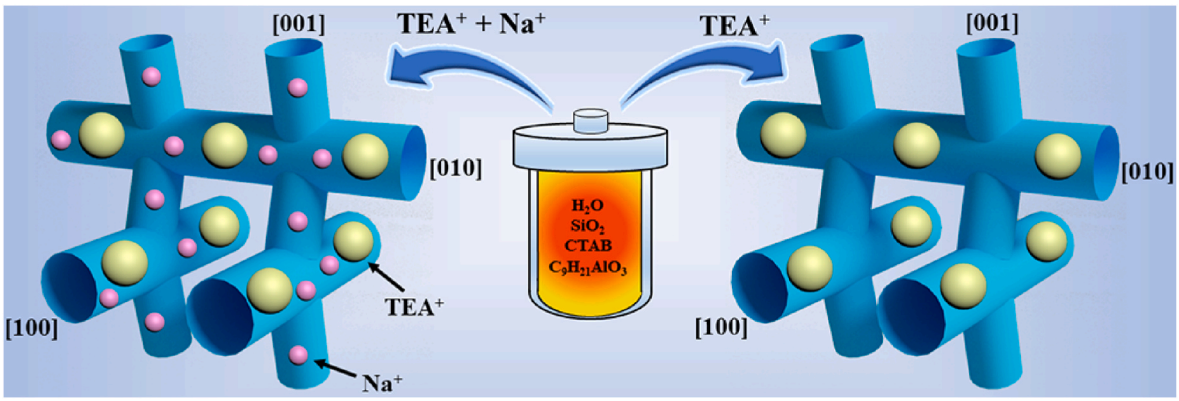

Scheme 1. The location of TEA^+ and Na^+ in the 12-MR pore channels of Beta zeolite.

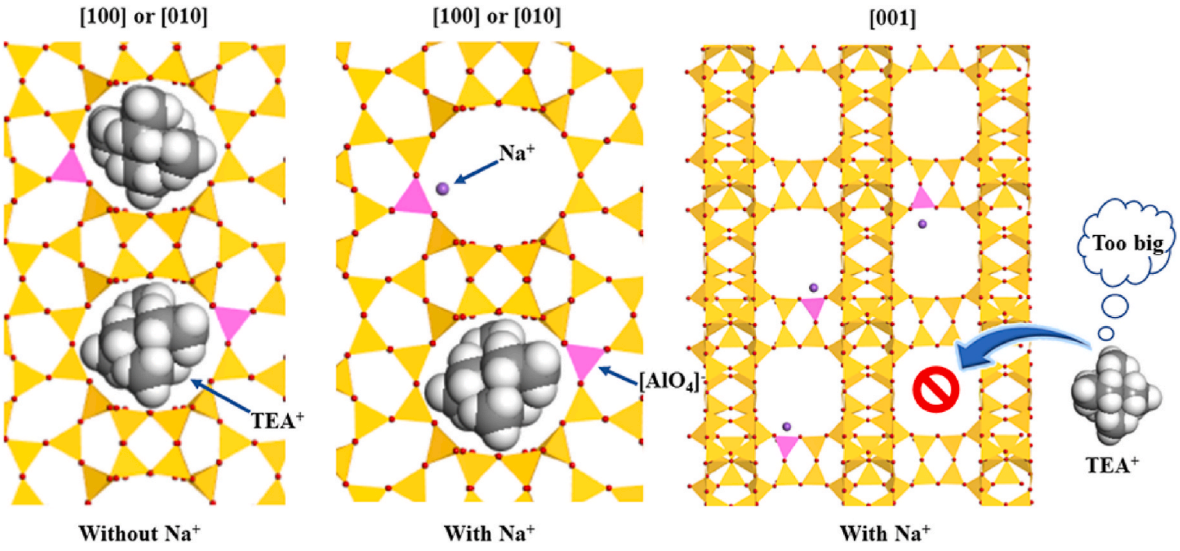

Scheme 2. Schematic illustration of the steric effect between TEA^+/Na^+ with 12 MR pore channels of Beta zeolite combined with controlled distribution of Al species.

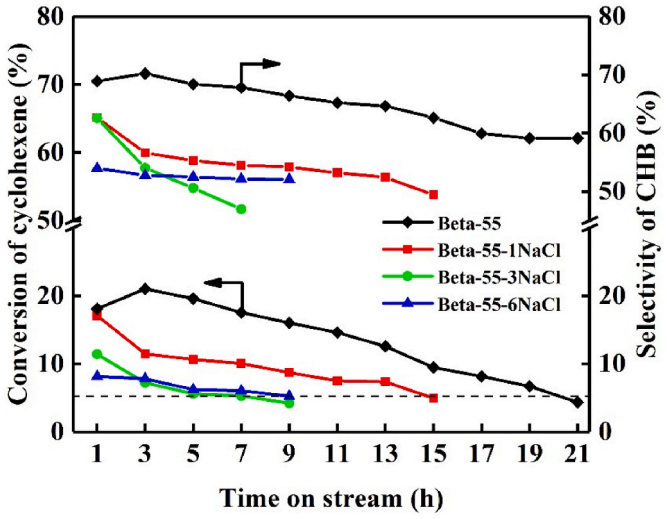

Fig. 5. Catalytic performance of alkylation for the resultant Beta55 and Beta-55-xNaCl. (Experimental conditions: benzene/cyclohexene mole ratio = 20; T = 353 K; P = 0.1 MPa; WHSV = 12 h^{-1}).

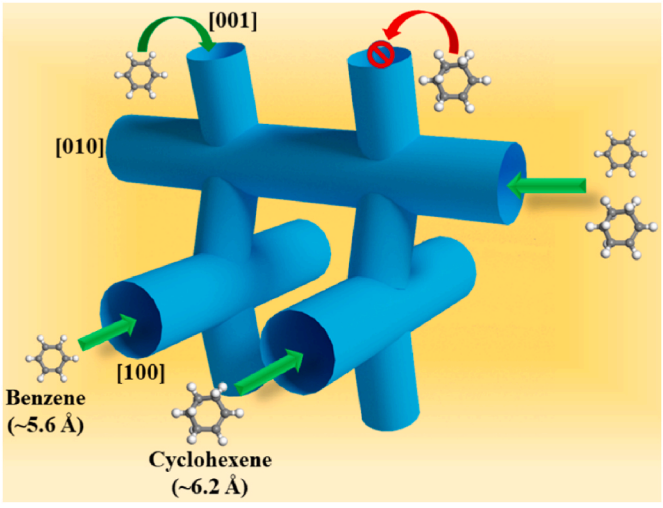

Scheme 3. Schematic diagram of the distribution of benzene and cyclohexene in the 12-MR pore channels of Beta zeolite.

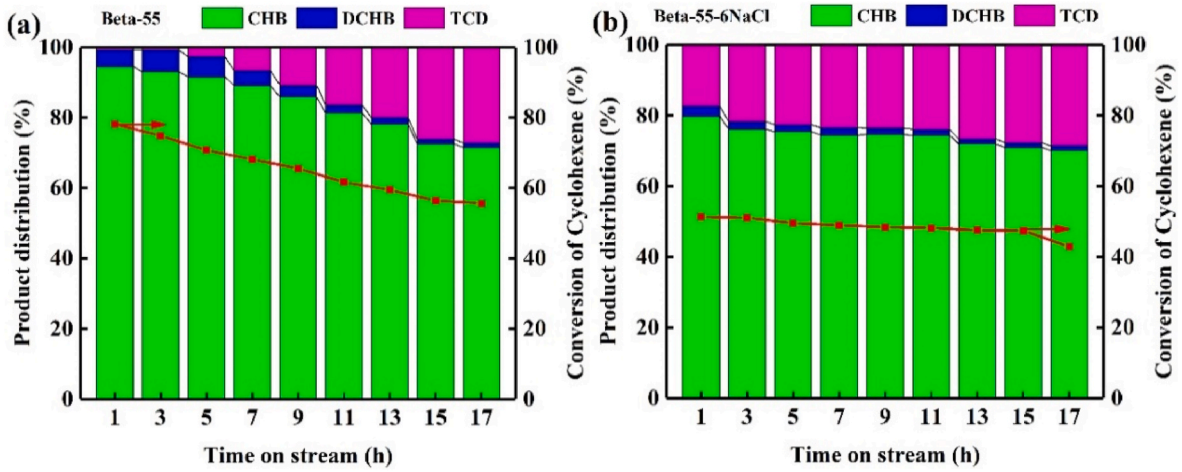

Fig. 6. Catalytic activity and product distribution in the alkylation over (a) Beta-55 and (b) Beta-55-6NaCl. (Experimental conditions: benzene/cyclohexene mole ratio = 20; T = 353 K; P = 0.1 MPa; WHSV = 2 h^{-1}).

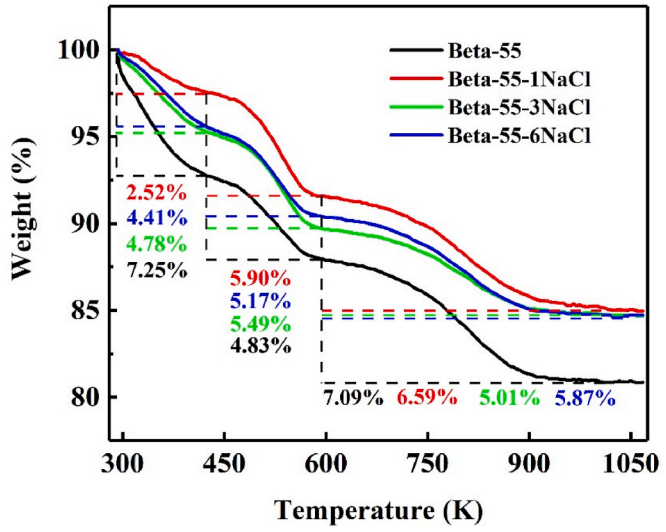

Fig. 7. Thermogravimetric (TG) curves of various spent Beta zeolites.

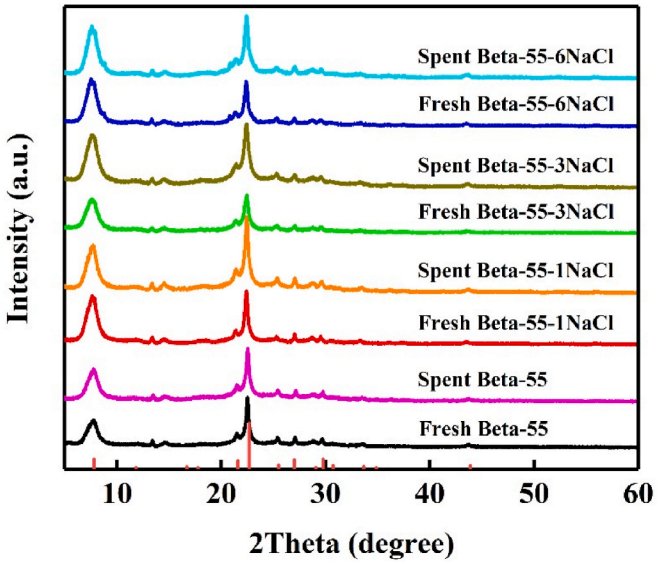

Fig. 8. XRD patterns of various catalysts before and after catalytic reactions.

Table 3
Coke deposit of resultant Beta zeolites.

Catalysts	soft coke[a] (g/g_0 cat) × 10^{-2}	hard coke[b] (g/g_0 cat) × 10^{-2}	Average coke rate ($mg{\cdot}g_0^{-1} \cdot h^{-1}$ cat)
Beta-55	4.83	7.09	4.13
Beta-55-1NaCl	5.90	6.59	5.17
Beta-55-3NaCl	5.49	5.01	6.57
Beta-55-6NaCl	5.17	5.87	7.70

zeolites in the alkylation, the spent Beta zeolites were directly regenerated by calcining them under air atmosphere. Fig. 8 illustrated the XRD patterns of fresh and regenerated Beta zeolites, all catalysts showed typical characteristic diffraction peaks of Beta zeolite, and the intensities of diffraction peak for obtained samples before and after the catalytic reactions did not change significantly, indicating that the obtained Beta zeolites possessed excellent stability.

Furthermore, the catalytic performances of typical regenerated Beta-55 and Beta-55-6NaCl were tested, and their catalytic data were illustrated in Fig. 9. It is evident that the regenerated Beta-55-6NaCl showed excellent regeneration behavior with a slight decrease in lifetime, while the regenerated Beta-55 exhibited inferior catalytic properties compared with fresh Beta-55, because Beta-55 possessed the highest amount of hard coke (Table 3), which was more difficult to remove in the regeneration process, leading to inferior regeneration property.

4. Conclusion

In conclusion, a facile strategy was developed to synthesize hierarchical Beta zeolites with precisely controlled distribution of Brønsted acidic sites in different three-dimension 12 MR pore channels of Beta zeolite by adjusting the content of Na^+ species in crystallization system, the fraction of Brønsted acid sites in the *a*- and *b*-axis channels of resultant Beta-55 was about 99%, while the proportion of Brønsted acid sites in the *a*-axis and *b*-axis channels of Beta-55-*x*NaCl gradually decreased in the order of Beta-55-1NaCl > Beta-55-3NaCl > Beta-55-6NaCl with increasing the content of Na^+ species in the crystallization system, indicating that the present strategy was an efficient method to regulate the position of Brønsted acid sites of Beta zeolite. In addition, the Beta-55 without Na^+ species exhibited extraordinary catalytic performances in the alkylation of benzene with cyclohexene such as the

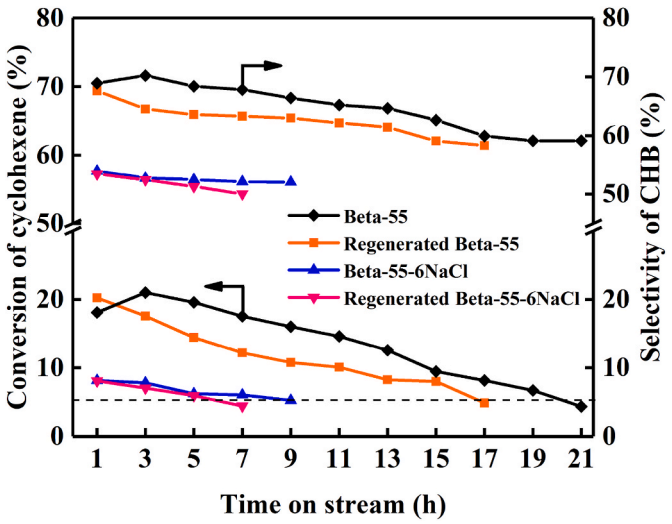

Fig. 9. Catalytic performance of alkylation for fresh and regenerated Beta-55 and Beta-55-xNaCl. (Experimental conditions: benzene/cyclohexene mole ratio = 20; T = 353 K; P = 0.1 MPa; WHSV = 12 h^{-1}).

highest activity, selectivity of cyclohexylbenzene and the longest lifetime. Additionally, the obtained Beta zeolites also exhibited excellent regeneration performance, which was decisive for the practical utilization of Beta zeolites in the alkylation of benzene with cyclohexene.

CRediT authorship contribution statement

Yeqing Huang: Data curation, Writing – original draft. **Manna Wang:** Conceptualization, Methodology, Software. **Yi Huang:** Visualization, Investigation. **Jin Shang:** Software, Validation. **Baoyu Liu:** Supervision, Writing – review & editing.

Declaration of competing interest

The authors declare that they have no known competing financial interests or personal relationships that could have appeared to influence the work reported in this paper.

Data availability

Data will be made available on request.

Acknowledgments

This work was supported by the National Natural Science Foundation of China (No. 21978055, 22278090), Natural Science Foundation of Guangdong Province, China (No. 2022A1515012088), the Science and Technology Planning Project of Guangdong Province, China (No. 2022A0505050073, 2022A0505030013).

References

[1] M. Fanfei, D. Linhui, M. Wei, D. Yuansheng, Q. Jun, High efficiency catalyst of modified Y molecular sieve by rare earth La3+ catalyzed the synthesis of cyclohexylbenzene from benzene and cyclohexene, Catal. Lett. 152 (2022) 745–754, https://doi.org/10.1007/s10562-021-03676-8.
[2] J. Fahy, D.L. Trimm, D.J. Cookson, Four component catalysis for the hydroalkylation of benzene to cyclohexyl benzene, Appl. Catal. A: Gen. 211 (2001) 259–268, https://doi.org/10.1016/S0926-860X(00)00872-3.
[3] N. Iwayasu, H. Honbou, T. Horiba, Overcharge protection effect and reaction mechanism of cyclohexylbenzene for lithium ion batteries, J. Power Sources 196 (2011) 3881–3886, https://doi.org/10.1016/j.jpowsour.2010.12.082.
[4] H. Lee, S. Kim, J. Jeon, J.-J. Cho, Proton and hydrogen formation by cyclohexyl benzene during overcharge of Li-ion batteries, J. Power Sources 173 (2007) 972–978, https://doi.org/10.1016/j.jpowsour.2007.08.061.
[5] M.Q. Xu, L.D. Xing, W.S. Li, X.X. Zuo, D. Shu, G.L. Li, Application of cyclohexyl benzene as electrolyte additive for overcharge protection of lithium ion battery, J. Power Sources 184 (2008) 427–431, https://doi.org/10.1016/j.jpowsour.2008.03.036.
[6] C.E. Song, W.H. Shim, E.J. Roh, J.H. Choi, Scandium triflate immobilised in ionic liquids: a novel and recyclable catalytic system for Friedel–Crafts alkylation of aromatic compounds with alkenes, Chem. Commun. (2000) 1695–1696, https://doi.org/10.1039/B005335J.
[7] C. Perego, P. Ingallina, Recent advances in the industrial alkylation of aromatics: new catalysts and new processes, Catal. Today 73 (2002) 3–22, https://doi.org/10.1016/S0920-5861(01)00511-9.
[8] P.S. Bárcia, J.A.C. Silva, A.E. Rodrigues, Adsorption equilibrium and kinetics of branched hexane isomers in pellets of BETA zeolite, Microporous Mesoporous Mater. 79 (2005) 145–163, https://doi.org/10.1016/j.micromeso.2004.10.037.
[9] X. Ji, Z. An, X. Yang, A memory diffusion model for molecular anisotropic diffusion in siliceous β-zeolite, J. Mol. Model. 22 (2016) 38, https://doi.org/10.1007/s00894-016-2911-6.
[10] Z. Yan, D. Chen, L. Huang, J. Liu, H. Fu, Y. Xiao, S. Li, A theoretical insight into diffusion mechanism of benzene-methanol alkylation reaction in ZSM-5 zeolite, Microporous Mesoporous Mater. 337 (2022), 111926, https://doi.org/10.1016/j.micromeso.2022.111926.
[11] J. Jae, G.A. Tompsett, A.J. Foster, K.D. Hammond, S.M. Auerbach, R.F. Lobo, G. W. Huber, Investigation into the shape selectivity of zeolite catalysts for biomass conversion, J. Catal. 279 (2011) 257–268, https://doi.org/10.1016/j.jcat.2011.01.019.
[12] S. Li, Z. Zhao, R. Zhao, D. Zhou, W. Zhang, Aluminum location and acid strength in an aluminum-rich beta zeolite catalyst: a combined density functional theory and solid-state NMR study, ChemCatChem 9 (2017) 1494–1502, https://doi.org/10.1002/cctc.201601623.
[13] W. Wang, W. Zhang, Y. Chen, X. Wen, H. Li, D. Yuan, Q. Guo, S. Ren, X. Pang, B. Shen, Mild-acid-assisted thermal or hydrothermal dealumination of zeolite beta, its regulation to Al distribution and catalytic cracking performance to hydrocarbons, J. Catal. 362 (2018) 94–105, https://doi.org/10.1016/j.jcat.2018.03.002.
[14] J. Dědeček, E. Tabor, S. Sklenak, Tuning the aluminum distribution in zeolites to increase their performance in acid-catalyzed reactions, ChemSusChem 12 (2019) 556–576, https://doi.org/10.1002/cssc.201801959.
[15] K. Yuan, X. Jia, S. Wang, S. Fan, S. He, P. Wang, Z. Qin, M. Dong, W. Fan, J. Wang, Regulating the distribution of acid sites in ZSM-11 zeolite with different halogen anions to enhance its catalytic performance in the conversion of methanol to olefins, Microporous Mesoporous Mater. 341 (2022), 112051, https://doi.org/10.1016/j.micromeso.2022.112051.
[16] R. Zhao, Z. Zhao, S. Li, W. Zhang, Insights into the correlation of aluminum distribution and Brönsted acidity in H-beta zeolites from solid-state NMR spectroscopy and DFT calculations, J. Phys. Chem. Lett. 8 (2017) 2323–2327, https://doi.org/10.1021/acs.jpclett.7b00711.
[17] A. Palčić, V. Valtchev, Analysis and control of acid sites in zeolites, Appl. Catal. A: Gen. 606 (2020), 117795, https://doi.org/10.1016/j.apcata.2020.117795.
[18] A. Abraham, S.-H. Lee, C.-H. Shin, S. Bong Hong, R. Prins, J.A. van Bokhoven, Influence of framework silicon to aluminium ratio on aluminium coordination and distribution in zeolite Beta investigated by 27Al MAS and 27Al MQ MAS NMR, Phys. Chem. Chem. Phys. 6 (2004) 3031–3036, https://doi.org/10.1039/B401235F.
[19] X. Zhao, L. Wang, J. Li, S. Xu, W. Zhang, Y. Wei, X. Guo, P. Tian, Z. Liu, Investigation of methanol conversion over high-Si beta zeolites and the reaction mechanism of their high propene selectivity, Catal. Sci. Technol. 7 (2017) 5882–5892, https://doi.org/10.1039/C7CY01804E.
[20] R. Barakov, N. Shcherban, P. Yaremov, I. Bezverkhyy, V. Tsyrina, M. Opanasenko, Hierarchical Beta zeolites obtained in concentrated reaction mixtures as catalysts in tetrahydropyranylation of alcohols, Appl. Catal. A: Gen. 594 (2020), 117380, https://doi.org/10.1016/j.apcata.2019.117380.
[21] C. Yang, Q. Xu, Aluminated zeolites β and their properties Part 1.—alumination of zeolites β, J. Chem. Soc., Faraday Trans. 93 (1997) 1675–1680, https://doi.org/10.1039/A606807C.
[22] A. Omegna, M. Haouas, G. Pirngruber, R. Prins, 11-P-28 - alumination of siliceous zeolites, in: A. Galarneau, F. Fajula, F. Di Renzo, J. Vedrine (Eds.), Studies in Surface Science and Catalysis, vol. 135, Elsevier, 2001, p. 215, https://doi.org/10.1016/S0167-2991(01)81433-6.
[23] N. Jappar, Q. Xia, T. Tatsumi, Oxidation activity of Ti-beta synthesized by a dry-gel conversion method, J. Catal. 180 (1998) 132–141, https://doi.org/10.1006/jcat.1998.2266.
[24] A. Corma, L.T. Nemeth, M. Renz, S. Valencia, Sn-zeolite beta as a heterogeneous chemoselective catalyst for Baeyer–Villiger oxidations, Nature 412 (2001) 423–425, https://doi.org/10.1038/35086546.
[25] B. Tang, W. Dai, X. Sun, N. Guan, L. Li, M. Hunger, A procedure for the preparation of Ti-Beta zeolites for catalytic epoxidation with hydrogen peroxide, Green Chem. 16 (2014) 2281–2291, https://doi.org/10.1039/C3GC42534G.
[26] M.H.M. Ahmed, O. Muraza, A. Galadima, M. Yoshioka, Z.H. Yamani, T. Yokoi, Choreographing boron-aluminum acidity and hierarchical porosity in *BEA zeolite by in-situ hydrothermal synthesis for a highly selective methanol to propylene catalyst, Microporous Mesoporous Mater. 273 (2019) 249–255, https://doi.org/10.1016/j.micromeso.2018.06.036.
[27] C. Yin, D. Tian, M. Xu, Y. Wei, X. Bao, Y. Chen, F. Wang, One-step synthesis of hierarchical mesoporous zeolite Beta microspheres from assembly of nanocrystals, J. Colloid Interface Sci. 397 (2013) 108–113, https://doi.org/10.1016/j.jcis.2013.02.006.

[28] Y. Huang, F. Xiong, Z. Zou, Y. Huang, Z. Zhao, B. Liu, J. Dong, Fabrication of β-zeolite nanocrystal aggregates for the alkylation of benzene and cyclohexene, Ind. Eng. Chem. Res. 62 (2023) 190–198, https://doi.org/10.1021/acs.iecr.2c03417.
[29] E. Schulman, W. Wu, D. Liu, Two-dimensional zeolite materials: structural and acidity properties, Materials 13 (2020), https://doi.org/10.3390/ma13081822.
[30] N.S. Nesterenko, F. Thibault-Starzyk, V. Montouillout, V.V. Yuschenko, C. Fernandez, J.P. Gilson, F. Fajula, I.I. Ivanova, Accessibility of the acid sites in dealuminated small-port mordenites studied by FTIR of co-adsorbed alkylpyridines and CO, Microporous Mesoporous Mater. 71 (2004) 157–166, https://doi.org/10.1016/j.micromeso.2004.03.028.
[31] H. Du, D.H. Olson, Surface acidic properties of A HMCM-22 zeolite: collidine poisoning and hydrocarbon adsorption studies, J. Phys. Chem. B 106 (2002) 395–400, https://doi.org/10.1021/jp013310s.
[32] S. Inagaki, K. Kamino, E. Kikuchi, M. Matsukata, Shape selectivity of MWW-type aluminosilicate zeolites in the alkylation of toluene with methanol, Appl. Catal. A: Gen. 318 (2007) 22–27, https://doi.org/10.1016/j.apcata.2006.10.036.
[33] S. Inagaki, S. Park, H. Yamazaki, J.N. Kondo, Y. Kubota, Investigation of the acidic nature of MCM-68 zeolite based on the adsorption of CO and bulky probe molecules, Microporous Mesoporous Mater. 272 (2018) 16–23, https://doi.org/10.1016/j.micromeso.2018.06.001.
[34] W. Hao, W. Zhang, Z. Guo, J. Ma, R. Li, Mesoporous beta zeolite catalysts for benzylation of naphthalene: effect of pore structure and acidity, Catalysts 8 (2018), https://doi.org/10.3390/catal8110504.
[35] N.S. Nesterenko, F. Thibault-Starzyk, V. Montouilliout, V.V. Yushchenko, C. Fernandez, J.P. Gilson, F. Fajula, I.I. Ivanova, The use of the consecutive adsorption of pyridine bases and carbon monoxide in the IR spectroscopic study of the accessibility of acid sites in microporous/mesoporous materials, Kinet. Catal. 47 (2006) 40–48, https://doi.org/10.1134/S0023158406010071.
[36] S. Abello, A. Bonilla, J. Perez-Ramirez, Mesoporous ZSM-5 zeolite catalysts prepared by desilication with organic hydroxides and comparison with NaOH leaching, Appl. Catal. A: Gen. 364 (2009) 191–198, https://doi.org/10.1016/j.apcata.2009.05.055.